Proceedings of 5th International Conference CNDGS'2026
ISSN 2669-2023 (print) / ISSN 2538-8959 (on-line) / **https://doi.org/10.47459/cndcgs.2026.9**

Terrain-Atmosphere Coupled Radar Detectability Mapping for Military Low-Level Air Maneuver

Petr PLÍVA[1]*, Lenka ROUČKOVÁ[1], Alžběta SCHNEIDROVÁ[1], Vladimír KOVAŘÍK[1], Jaromír ČAPEK[1]

[1]*Department of Military Geography and Meteorology, Faculty of Military Technology, University of Defence, Address: Kounicova 65, 662 10 Brno, Czech Republic*

*Correspondence: *petr.pliva@unob.cz*

Abstract

Military low-level air maneuver in contested environments is constrained by adversary radar surveillance and the need to minimize exposure while remaining terrain- and mission-feasible. Although terrain masking reduces direct line-of-sight (LOS) to a radar, detectability cannot be assessed from geometry alone, as it also depends on the radar energy budget, receiver noise, processing gain, and the adopted detection criterion. This paper presents a reproducible GIS-oriented workflow that couples LOS-based masking products, including visibility and minimal visible altitude above ground level (AGL), with an energy-based detectability model expressed through signal-to-noise ratio (SNR) and probability of detection (PD). The workflow further incorporates scenario-dependent atmospheric modifiers representing gaseous attenuation, rain attenuation, and refractivity-driven propagation effects, while retaining the possibility of higher-fidelity propagation modelling where required. In addition to 2D exposure layers, the approach supports constrained low-exposure route generation and optional 3D voxel-based representations of detectability in the near-ground layer. A case study in the Brno area demonstrates the generation of LOS and altitude-margin products, SNR/PD raster layers, and example low-exposure corridors derived from raster threat masks. The results show that radar exposure is highly sensitive to terrain, altitude, and environmental assumptions, and that the proposed workflow provides a transferable decision-support framework for comparative analysis of low-level operations in contested airspace.

KEY WORDS: *Atmospheric propagation; Detectability-constrained routing; Probability of detection; Radar exposure assessment; Terrain masking*

Citation: Plíva, P.; Roučková, L.; Schneidrová, A.; Kovařík, V.; Čapek, V. Terrain-Atmosphere Coupled Radar Detectability Mapping for Military Low-Lever Air Manoeuvre. In Proceedings of the Challenges to National Defence in Contemporary Geopolitical Situation, Brno, Czech Republic, 7-10 September 2026. ISSN 2538-8959, https://doi.org/10.47459/cndcgs.2026.9

1. Introduction

Contested airspace operations require military air assets to maneuver under persistent adversary surveillance and within potential threat engagement envelopes. In missions such as tactical penetration, escort, time-sensitive targeting support, special operations, or low-signature ingress and egress, low-level flight may exploit terrain masking to reduce exposure to hostile sensors. However, terrain masking alone does not guarantee survivability. The detectability of an airborne target is governed not only by line-of-sight (LOS) geometry, but also by radar performance margins, processing assumptions, and the statistical decision criterion that links signal-to-noise ratio (SNR) to probability of detection (PD) under a specified probability of false alarm (PFA) [1-4]. Mission planning and post-mission analysis therefore require quantitative products that distinguish geometric exposure from actual detection likelihood.

Many geospatial products used in operational planning remain primarily viewshed-based, providing binary visibility or simplified exposure indices. Viewshed methods are mature, computationally efficient, and scalable for raster-based terrain analysis [2], while recent parallel and GPU-based approaches have further improved their applicability to large-scale and multi-viewpoint problems [5]. Nevertheless, binary visibility alone cannot capture energy-limited detection regimes, variations in detection thresholds, or weather- and propagation-dependent losses that influence SNR and, consequently, PD.

Peer-review under responsibility of General Jonas Žemaitis Miltitary Academy of Lithuania and University of Defence, Czech Republic.

A more operationally relevant framework must therefore combine terrain masking with a detection-theory-consistent transformation from SNR → PD [3,4].

This paper contributes a reproducible workflow for radar exposure analysis tailored to military low-level air maneuver. The approach integrates:

1. terrain-based LOS visibility ("visible"),
2. the minimum visible altitude above ground level, which provides an operationally interpretable measure of terrain shielding,
3. spatial SNR modelling and PD mapping,
4. low-exposure corridor derivation via constrained shortest-path routing,
5. optional 3D voxel coverage products for volumetric interpretation [6].

Meteorological influences are incorporated as scenario-dependent modifiers in the propagation and detectability chain using ITU-R recommendations [7-9], while the framework also allows extension toward higher-fidelity parabolic-equation-based modelling for complex propagation environments [10, 11].

2. Data and Area of Interest

Terrain and obstacle structure are represented using a Digital Surface Model (DSM) rather than a bare-earth DEM/DTM, such as buildings and vegetation, which may significantly influence near-ground masking and corridor structure [12-14]. This choice allows the analysis to account not only for topographic relief, but also for above-ground surface objects, such as buildings and vegetation, which may significantly influence near-ground masking and corridor structure. The study area is discretized into a raster grid defined by the spatial resolution of the DSM. The radar scenario is specified by radar position, antenna height above the local surface, maximum analysis radius, and the set of parameters required for subsequent detectability modelling.

The area of interest (AOI) located in Brno (Czech Republic) is defined as a circular region with radius $R_{max} = 3000$ m around the radar site. The radar position was initially specified in geographic coordinates and corresponds approximately to $(\varphi, \lambda) \approx (49.21703°\text{N}, 16.61242°\text{E})$. The AOI represents a heterogeneous urban and peri-urban environment in which radar exposure is controlled by the combined effects of rolling relief, ridge-and-valley morphology, and surface obstacles. As a result, the use of a DSM is particularly appropriate, since it captures the near-ground shielding conditions relevant to low-level air maneuver more realistically than a bare-earth terrain model.

3. Methodology

The proposed approach implements a reproducible, configuration-driven GIS workflow for assessing radar exposure in support of military low-level air maneuver analysis. The workflow is founded on two complementary principles - geometric masking, which determines LOS availability as a function of the surface model, and energy-based detectability, which determines whether a geometrically exposed target is likely to be detected under a specified decision criterion. This separation is essential because LOS visibility alone does not uniquely determine detectability; the latter depends on the signal-to-noise ratio (SNR), processing assumptions, and the probability-of-detection mapping at a fixed probability of false alarm P_{FA} [1, 3, 4]. Raster-based LOS modelling provides computationally efficient masking layers over large areas [2,5], while detection theory provides a consistent framework for translating SNR into P_D [3,4]. The resulting products are subsequently operationalized through corridor extraction and optional volumetric (3D) representation [6, 14].

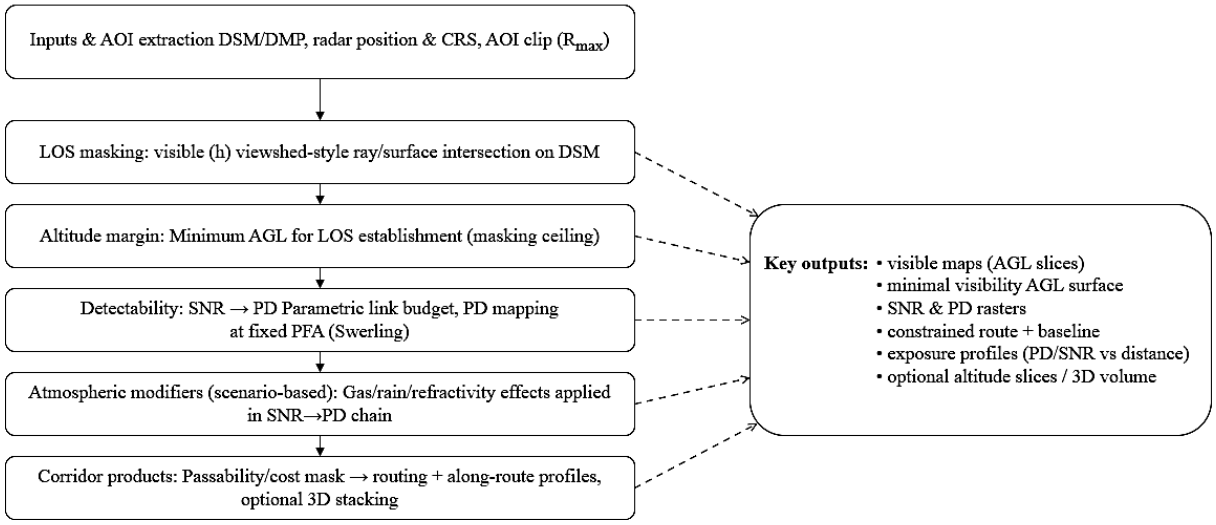

Fig. 1: Configuration-driven terrain–atmosphere coupled radar detectability workflow.

The overall processing chain is summarized in Fig. 1, highlighting the separation between geometric masking, energy-based detectability, atmospheric modifiers, and corridor extraction. By applying DEM generalization, the duration of the real-time route determination process avoiding impassable areas can be significantly reduced without compromising the accuracy required for military operations [15].

A DSM is used to represent the surface (relief plus above-ground objects) relevant to near-ground masking. The AOI is defined as a circular region around the radar site with $R_{\max}$. Radar coordinates are reprojected into the DSM coordinate reference system, and the DSM is clipped to the AOI to reduce computational cost while preserving all surface structures influencing LOS within $R_{\max}$. This clipping step ensured computational tractability for dense angular and range sampling while maintaining the spatial detail required for masking analysis in an urban and peri-urban environment. The geometric and sampling configuration adopted in the study is summarized in Table 1.

Table 1: Geometric and sampling parameters

Item	**Value**
Maximum range R_{max}	3000.00 m
Antenna height above local surface	1.00 m AGL
Azimuth step $\Delta\alpha$	0.01°
Range step Δr	10.00 m
Earth curvature / refraction	Enabled (effective Earth radius k = 4/3)

LOS visibility was computed by ray/surface intersection on the raster DSM (viewshed-style modelling) [2,5]. For each selected altitude AGL, a binary visibility layer, hereafter referred to as visible, was produced to indicate whether LOS existed between the radar and the target location at that altitude. This binary LOS layer represents the baseline geometric exposure product and provides the necessary reference for distinguishing purely geometric masking from energy-limited detectability

To avoid repeated recomputation of viewsheds for multiple altitude levels and to capture altitude sensitivity in a compact form, the workflow also derived the minimum visible altitude above ground level (h_{min}). For each horizontal location, this layer defines the minimum altitude above the local surface at which LOS to the radar becomes available. Operationally, it can be interpreted as a spatially explicit "*masking ceiling"*, supporting rapid assessment of how small AGL changes alter exposure conditions. This product is particularly relevant in the near-ground layer, where transitions between masked and exposed states are often discontinuous with altitude and therefore cannot be adequately described by a single viewshed alone.

For each AGL slice, the workflow estimates spatial SNR using a parametric radar link-budget model and converts SNR to probability of detection P_D under a specified decision criterion (fixed P_{FA}) and target fluctuation assumptions (Swerling model) [3,4]. The detection and processing parameters used in the scenario are reported in Table 2. P_D is a mission-relevant metric enabling consistent spatial comparison and threshold-based exposure zoning; it explicitly separates geometrically visible space from and space associated with a high likelihood of detection.

Table 2: Detection and processing parameters

Item	**Value**
Carrier frequency f	10.00 GHz
Bandwidth B	20.00 MHz
Transmit power P_t	20.00 kW
Antenna gain G	40.00 dBi
System losses L	6.00 dB
Noise figure NF	6.00 dB
Assumed $RCS\ \sigma$	0.01 m²
Processing gain	20.00 dB
Probability of false alarm P_{FA}	10.00^{-6}
Number of pulses N_{pulses}	16.00

Meteorological and atmospheric influences were represented as scenario-dependent modifiers applied in the SNR→P_D chain, while the geometric LOS stage remains unchanged. This stage supports sensitivity analysis to gaseous attenuation, rain attenuation, and refractivity-driven effects following ITU-R recommendations [7-9], with a pathway to higher-fidelity propagation modelling (e.g., parabolic-equation approaches) when required [10]. Atmospheric effects were included because

they may materially shift detectability margins and alter corridor feasibility even where the underlying LOS geometry remains unchanged.

Finally, the exposure layers were transformed into constraints or cost fields for corridor extraction using shortest-path routing on a raster grid. A passability mask was derived from LOS visibility and/or detectability thresholds, yielding the shortest feasible corridor between defined endpoints under explicit exposure constraints. In addition, exposure products could be stacked across altitude to form an optional volumetric representation, supporting interpretation of feasible altitude bands and corridor connectivity in three dimensions [6]. In this way, the workflow converts map-based exposure products into mission-oriented outputs that quantify survivability–efficiency trade-offs under clearly defined assumptions.

To resolve the near-ground regime in sufficient detail, all exposure products were evaluated on the following AGL slices: $h \in \{0, 1, 2, \ldots 10, 15, 20, 25, 50, 100, 200\}$ m.

4. Results and Discussion

The results confirm that radar exposure in the Brno AOI is governed by the coupled interaction of surface-driven LOS masking captured by the DSM and energy-limited detectability expressed through SNR and P_D. The strongest geometric result is provided by the h_{min} product, which maps the minimum altitude required for LOS establishment at each horizontal location. As shown in Fig. 2, this quantity is highly heterogeneous across the AOI, with low values in areas where even a modest altitude increase leads to exposure and markedly higher values in sectors where shielding remains robust up to substantially greater heights. In operational terms, this layer can be interpreted as a spatially explicit masking ceiling and therefore provides a compact descriptor of altitude margins relevant to low-level maneuver.

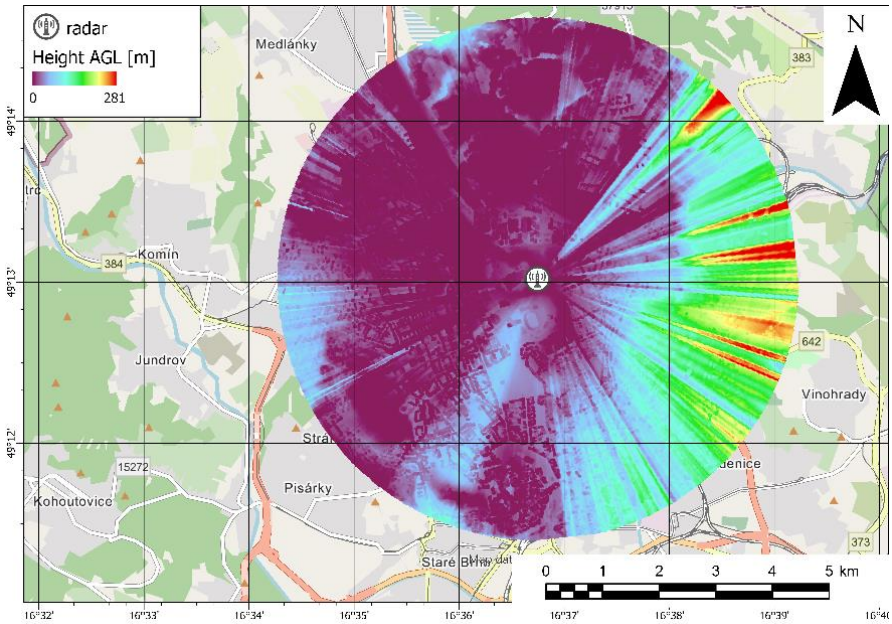

Fig. 2: Spatial distribution of minimum visible altitude AGL (h_{min}) in the Brno AOI. The raster expresses the minimum AGL required to establish line-of-sight to the radar and can be interpreted as a spatially explicit masking ceiling.

Across the AOI, the mean value of h_{min} is 40.35 m, while the median is 19.06 m, indicating a strongly asymmetric distribution in which a large proportion of the area becomes visible after relatively small altitude increases, whereas a smaller but operationally important fraction remains shielded up to substantially greater heights. This confirms that the near-ground environment contains both fragile and robust masking zones and supports the interpretation of h_{min} as an operationally meaningful altitude-margin product.

The statistical structure of this product is further illustrated by the histogram of h_{min} product in Fig. 3. The distribution is strongly right-skewed, indicating that a large proportion of the area becomes visible after relatively small altitude increases, while a smaller but operationally significant fraction remains masked until substantially higher AGL. This confirms that the near-ground environment contains both fragile and robust shielding zones and that a single binary visibility product is insufficient for describing altitude-sensitive exposure conditions.

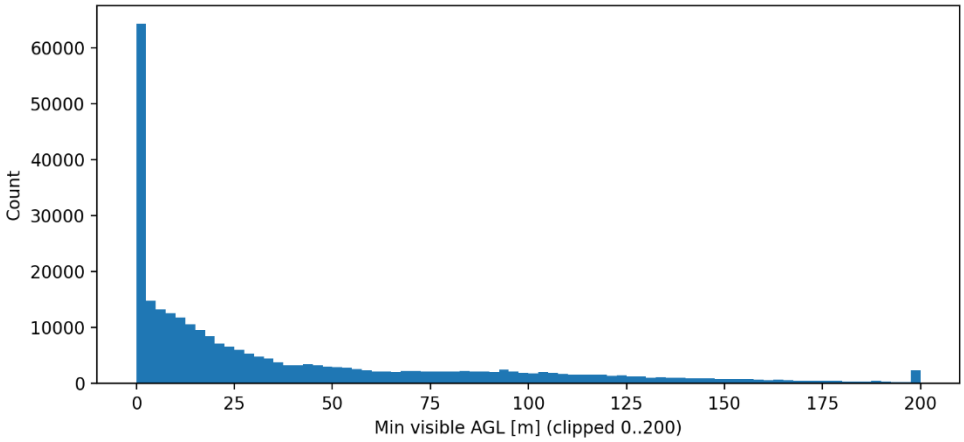

Fig. 3: Histogram of h_{min} values within the analyzed footprint, illustrating the strongly right-skewed distribution of altitude margins required for LOS establishment.

The strong altitude dependence of the analyzed domain is quantified by the LOS coverage curve in Fig. 4, which shows a rapid increase in visible area within the lowest tens of meters above ground, followed by a more gradual approach towards near-complete visibility at higher AGL. This behavior indicates that transitions between masked and exposed states are distinctly non-linear with altitude. Such non-linearity is also evident in the representative binary visibility maps in Fig. 5, where connectivity of visible and masked space changes substantially between selected AGL levels. Together, these products demonstrate that low-level exposure cannot be interpreted from a single flight height alone and justify the use of altitude-sliced analysis.

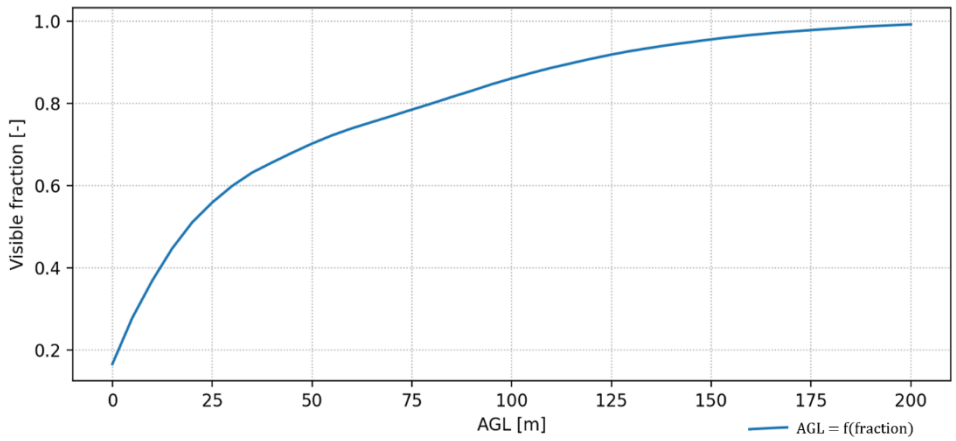

Fig. 4: Fraction of LOS-visible area as a function of AGL, demonstrating the rapid increase in exposure in the lowest tens of meters above ground and the subsequent gradual approach to near-complete visibility.

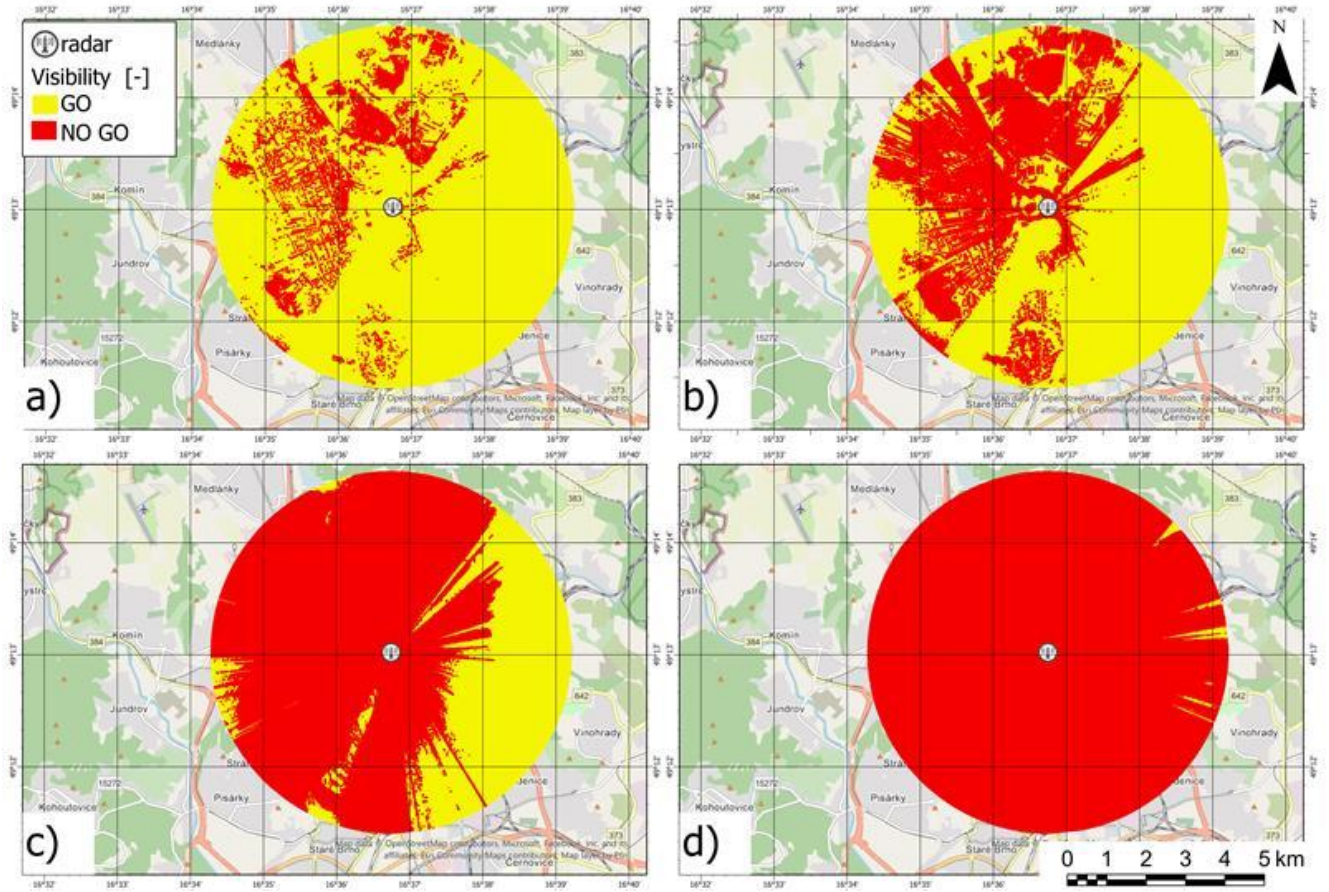

Fig. 5: Representative binary LOS visibility maps at AGL levels a) is 0 m, b) is 10 m, c) is 50 m and d) is 200 m, illustrating the non-linear transition between masked and exposed space in the near-ground layer.

The visible fraction increases from 0.17 at 0.00 m to 0.28 at 5.00 m, 0.37 at 10.00 m, 0.56 at 25.00 m, 0.70 at 50.00 m, 0.86 at 100.00 m, and 0.99 at 200.00 m AGL. This progression shows that the rapid expansion of exposed space occurs within the lowest tens of meters above ground, after which the increase becomes more gradual as the AOI approaches near-complete visibility.

The energy-based stage refines this geometric interpretation by estimating the spatial distribution of SNR and PD. The representative SNR raster in Fig. 6 shows a clear spatial gradient within the LOS-visible domain, with the highest values concentrated in the radar-proximal sector and progressively lower values towards more distant visible regions. This confirms that the model captures the expected range-driven degradation of detection margin. However, under the present baseline parameterization, the corresponding PD field in Fig. 7 is close to unity across most visible cells. In this configuration, detectability is effectively saturated within the LOS-visible domain, and the principal source of spatial discrimination remains the masking geometry rather than internal variation in PD. This result is nevertheless informative: it indicates that, for the selected radar configuration and analysis radius, once a target becomes visible, detection is highly likely. Consequently, the SNR/PD framework should be interpreted here primarily as a scenario-analysis capability, expected to become more discriminative under reduced radar performance, altered target assumptions, or adverse atmospheric conditions.

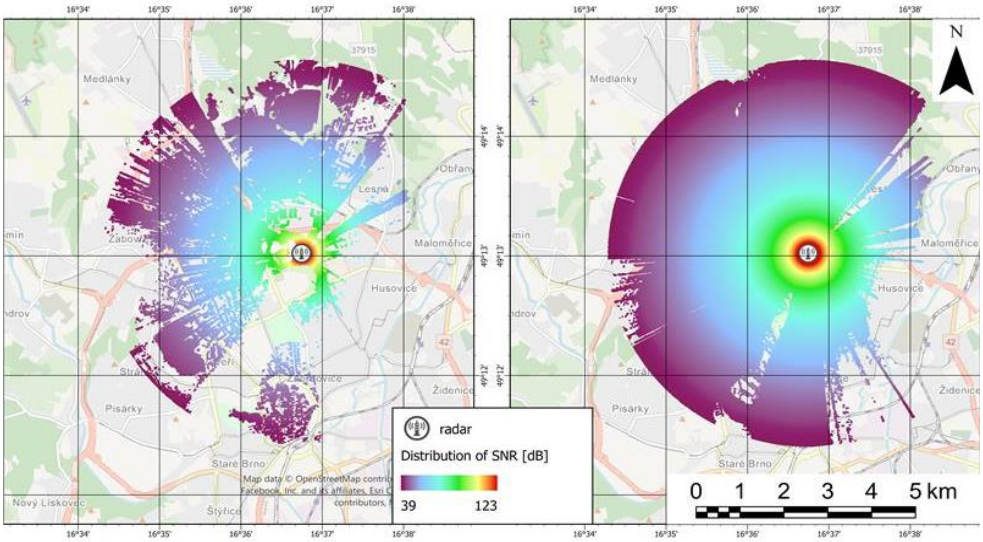

Fig. 6: Spatial distribution of SNR (dB) on the left map at 10.00 m and on the right map at 50.00 m AGL for the baseline radar configuration, showing range-driven degradation of detection margin within the LOS-visible domain.

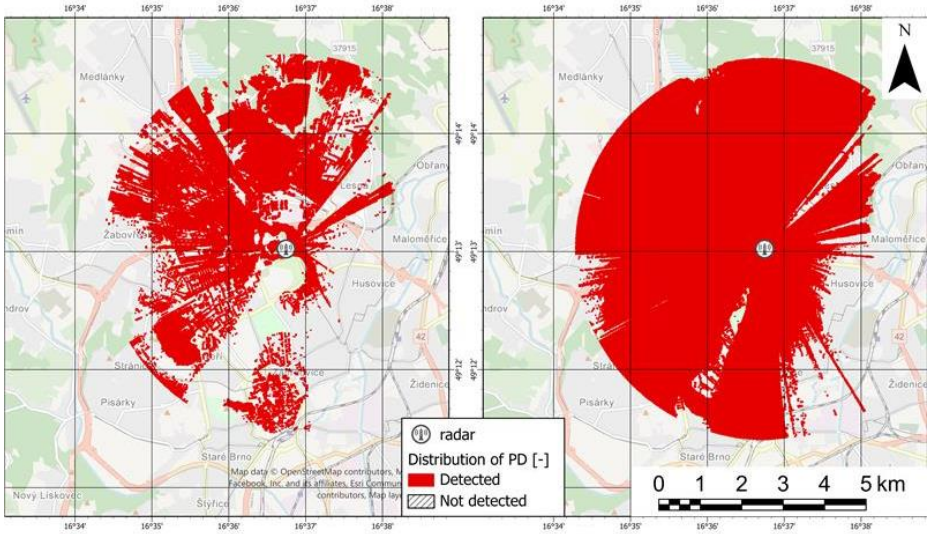

Fig. 7: Spatial distribution of PD on the left map at 10.00 m and on the right map at 50.00 m AGL under the baseline scenario. In the present configuration, PD approaches unity across most visible cells, indicating saturated detectability within the LOS-visible domain.

This trend is also reflected in the summary statistics. The mean SNR in visible cells is 50.14 dB at 5.00 m AGL, while the corresponding median SNR is 47.89 dB. With increasing altitude, the mean SNR decreases only moderately as progressively more distant visible cells are included in the exposed domain. By contrast, the probability of detection is effectively saturated in the baseline configuration: for all analyzed AGL levels, both the mean and median P_D in visible cells are equal to 1.00, and the fraction of visible cells with $P_D \geq 0.50$ is likewise 1.00. Under these conditions, the dominant source of spatial discrimination remains the masking geometry itself rather than internal variation in detectability.

The practical relevance of the workflow becomes most evident in the routing stage. By transforming the exposure layer into an explicit raster constraint, the model identifies feasible low-exposure corridors under a selected rule, such as non-visible space, a minimum visibility margin, or a prescribed detectability threshold. The resulting constrained route follows connected shielding structures and avoids sectors where exposure exceeds the permitted limit. Compared with an unconstrained baseline path, this route provides a direct measure of the survivability–efficiency trade-off. The along-route profile in Fig. 8 further reveals where the corridor approaches the limiting threshold and therefore where route robustness is weakest with respect to altitude deviation, navigation error, or environmental perturbation. In this way, the analysis moves beyond the question of whether a route exists and instead evaluates the relative resilience of that route under the chosen exposure assumptions.

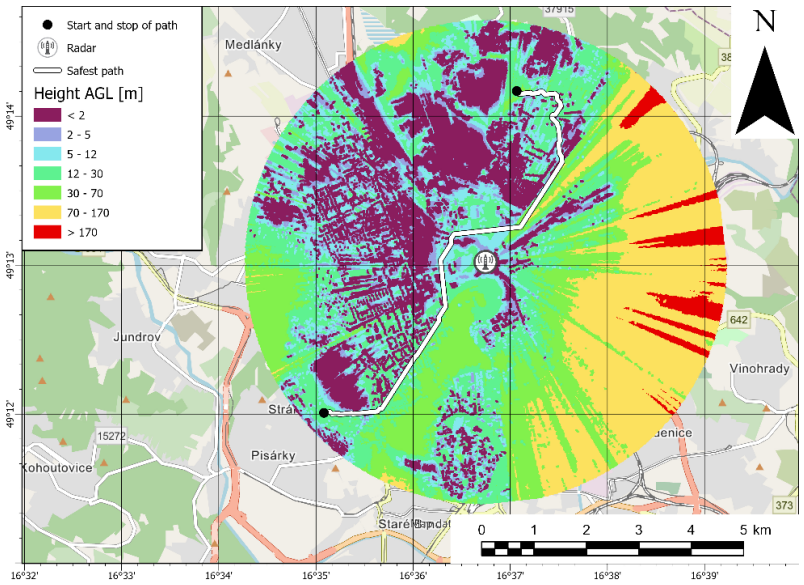

Fig. 8: Along-route exposure profile for the constrained corridor, showing the variation of PD, h_{min} and visibility margin with cumulative distance and identifying the most sensitive route segments.

The constrained corridor was derived from a raster mask retaining only cells with h_{min} > 5.00 m, i.e., locations that remain masked for a transit altitude of 5.00 m AGL. Compared with the straight-line baseline between the route endpoints, the constrained path length increased from 4.65 km to 6.52 km, corresponding to an increase of approximately 40.10%. This difference directly quantifies the survivability–efficiency trade-off imposed by the masking constraint. In this formulation, the along-route profile should be interpreted as a measure of masking robustness rather than detectability variation, because the baseline PD field is saturated within the visible domain. Segments where the route approaches the 5 m masking threshold indicate locations in which even modest altitude deviations may lead to loss of concealment. Accordingly, Fig. 8 identifies the most fragile parts of the corridor and complements the plan-view route map by highlighting where the selected 5 m transit remains operationally robust and where it becomes sensitive to perturbation. If atmospheric scenarios were evaluated, their effect should be presented as a sensitivity result rather than as an independent product. In that case, an additional figure may be used to show how gaseous attenuation, rain attenuation, or refractivity-driven propagation modifies detectability margins without changing the underlying LOS geometry. Such results would support the interpretation that corridor feasibility is scenario-dependent and that a single atmospheric state cannot fully characterize operational exposure.

Overall, the current results support three main conclusions. First, the near-ground exposure pattern in the Brno AOI is dominated by strongly structured DSM-driven masking. Second, h_{min} provides a particularly valuable operational descriptor because it summarizes altitude margins to LOS in a compact, spatially explicit form. Third, while the energy-based stage confirms the expected variation of SNR within visible space, the baseline PD products are largely saturated, indicating that the present configuration is geometry-dominated rather than detectability-differentiated. In this sense, the strongest contribution of the current case study lies in the geometric characterization of exposure and altitude margins, while the detectability framework provides the basis for more discriminative scenario-driven extensions.

This interpretation is consistent with the routing result at 5.00 m AGL, where feasibility is controlled primarily by the continuity of masked space rather than by internal variation in PD. In the present baseline scenario, the workflow therefore functions mainly as a geometry-driven exposure and corridor analysis, while the SNR/PD stage provides the methodological basis for more discriminative scenario comparisons under degraded radar performance or altered atmospheric condition

5. Conclusions

This paper presented a terrain–atmosphere coupled, GIS-oriented workflow for radar exposure assessment in the context of military low-level air maneuver in contested environments. The main contribution is the integration of DSM-based masking products-binary visibility and minimum visible altitude above ground level (h_{min}) – with an energy-based detectability framework expressed through SNR and PD. By combining geometric masking with detectability modelling, the proposed approach extends conventional visibility-only GIS analyses toward a more operationally relevant representation of radar exposure.

The Brno case study showed that the most informative results are currently provided by the geometric stage of the workflow. In particular, h_{min} proved to be a compact and operationally interpretable descriptor of altitude margins required for LOS establishment. The results further demonstrated that exposure in the near-ground layer is highly sensitive to altitude, with rapid and non-linear transitions between masked and exposed states in the lowest tens of meters above ground. Although the detectability stage confirmed the expected spatial variation of SNR within the visible domain, the corresponding PD field

was largely saturated under the baseline parameterization. Consequently, in the present scenario, exposure assessment and corridor feasibility are governed primarily by masking geometry rather than by internal variation in detection probability.

The workflow nevertheless provides a transferable basis for comparative analysis, including visibility and altitude-margin mapping, SNR/PD raster generation, and constrained corridor derivation from raster exposure masks. Its configuration-driven structure enables efficient adaptation to different sensors, areas of interest, environmental assumptions, and operational constraints. In this sense, the outputs are best understood as decision-support products for planning and analysis, rather than as direct substitutes for tactical judgement.

Further work should focus on systematic atmospheric scenario analysis, higher-fidelity propagation modelling where required, and extension of the routing stage toward weighted multi-objective optimization. Equally important is formal validation against reference models, controlled benchmarks, and, where feasible, field measurements. At present, the results should therefore be interpreted primarily as a comparative model-based assessment, since the workflow has not yet been validated through dedicated field trials.

Acknowledgements. The authors thank the editors and reviewers for their valuable comments, which helped improve the manuscript. The work was supported by the Ministry of Defence of the Czech Republic "Institutional support for the development of research organizations" – Military autonomous and robotic assets of the Military Faculty of Technology, University of Defence, Czech Republic (Project No: DZRO-FVT22-VAROPS) and by the Ministry of Education, Youth and Sports of the Czech Republic (Specific Research Project No: SV24-210/2).

References

1. Skolnik M. I. (1980). Introduction to radar systems (2. ed). MacGraw-Hill.
2. Franklin, R. (28/05/1994). Higher isn't Necessarily Better: Visibility Algorithms and Experiments. In (p. 22). https://wrfranklin.org/p/84-edinburgh-sdh94-higher-not-better.pdf
3. Mark A. Richards. (2005). Fundamentals of Radar Signal Processing. McGraw-Hill.
4. Kay, S. M. (1998). Fundamentals of statistical signal processing (Vol. II, Detection theory). Prentice Hall.
5. Xiao, T., Deng, J., Wen, C., & Gu, Q. (2024). Parallel algorithm for multi-viewpoint viewshed analysis on the GPU grounded in target cluster segmentation. International Journal Of Digital Earth, 17(1), 1-19. https://doi.org/10.1080/17538947.2024.2308707
6. Aleksandrov, M., Zlatanova, S., Kimmel, L., Barton, J., & Gorte, B. (2019). VOXEL-BASED VISIBILITY ANALYSIS FOR SAFETY ASSESSMENT OF URBAN ENVIRONMENTS. ISPRS Annals of the Photogrammetry, Remote Sensing and Spatial Information Sciences, IV-4/W8(W8:11-17), 11-17. https://doi.org/10.5194/isprs-annals-iv-4-w8-11-2019
7. RECOMMENDATION ITU-R P.676-13: Attenuation by atmospheric gases and related effects. (2022). https://www.itu.int/dms_pubrec/itu-r/rec/p/R-REC-P.838-3-200503-I!!PDF-E.pdf
8. RECOMMENDATION ITU-R P.838-3: Specific attenuation model for rain for use in prediction methods. (2005). https://www.itu.int/dms_pubrec/itu-r/rec/p/R-REC-P.838-3-200503-I!!PDF-E.pdf
9. RECOMMENDATION ITU-R P.453-14: The radio refractive index: its formula and refractivity data. (2022). https://www.itu.int/dms_pubrec/itu-r/rec/p/R-REC-P.453-14-201908-I!!PDF-E.pdf
10. Zhang, R., Wang, H., Wu, Z., Lin, L., & Zhao, Z. (2024). Prediction Method of Maximum Propagation Angle in Parabolic Equation Model over Irregular Terrain. *International Journal Of Antennas And Propagation, 2024*(1). https://doi.org/10.1155/2024/4988555
11. Kovařík, V., Plíva, P., Rybanský, M., & Polívka, P. (2025). Model creation in ArcGIS Pro ModelBuilder for automatic search of locations suitable for helicopter and airship landings. *2025 International Conference on Military Technologies (ICMT)*. IEEE, s. 1–6. https://doi.org/10.1109/icmt65201.2025.11061278.
12. Hubacek, M., Brenova, M., Ceplova, L., & Zerzan, P. (2014). Verification of Accuracy of the New Generation Elevation Models. http://aimt.unob.cz/articles/14_02/14_02%20%282%29.pdf.
13. Hubacek, M., Kratochvil, V., Zerzan, P., Ceplova, L., & Brenova, M. (2015). Accuracy of the new generation elevation models. *International Conference on Military Technologies (ICMT) 2015*. IEEE, 2015, s. 1–6. https://doi.org/10.1109/miltechs.2015.7153725. [cit. 2026-03-20]
14. Ge, J., Xiang, J., & Li, D. (2024). Online penetration trajectory planning using blind areas of network radar system for an unmanned combat aerial vehicle. *Aircraft Engineering And Aerospace Technology*, 96(10), 1321-1328. https://doi.org/10.1108/aeat-07-2024-0207
15. Dawid, W., Pokonieczny, K., & Wyszyński, M. (2024). Optimization of the Route Determination Process for the Purposes of Military Terrain Passability. *Advances in Military Technology*, 19(1), 5–23. ISSN 1802-2308. https://doi.org/10.3849/aimt.01865.